

Causality relations in the homogenization of metamaterials

Andrea Alù,^{1,*} Arthur D. Yaghjian,² Robert A. Shore,³ and Mário G. Silveirinha⁴

¹*Department of Electrical and Computer Engineering, 1 University Station C0803, The University of Texas at Austin, Austin, Texas 78712, USA*

²*Research Consultant, 115 Wright Road, Concord, Massachusetts 01742, USA*

³*AFRL/Ryha, Hanscom AFB, Massachusetts 01731, USA*

⁴*Department of Electrical Engineering, University of Coimbra, Instituto de Telecomunicações, Coimbra, Portugal*
(Received 22 April 2011; revised manuscript received 9 June 2011; published 26 August 2011)

We investigate the causality relations in homogenized metamaterial arrays and determine the reasons why metamaterial effective (bulk) constitutive parameters obtained using classic point-dipole approximations may violate basic causality conditions represented by the Kramers-Kronig relations. We show that noncausality is inherently introduced by the use of point-dipole approximations within Maxwell-Garnett homogenization procedures and that these artifacts become particularly significant for more densely packed arrays. In contrast we show that properly defined and exactly computed bulk constitutive parameters of periodic metamaterial arrays always satisfy causality for a fixed spatial frequency in a rigorous homogenization framework. Finally we show how the Maxwell-Garnett approach can be modified to effectively remove the noncausal effects.

DOI: [10.1103/PhysRevB.84.054305](https://doi.org/10.1103/PhysRevB.84.054305)

PACS number(s): 78.20.-e, 42.70.Qs, 41.20.Jb, 42.25.Bs

I. INTRODUCTION

The interest in metamaterials for a variety of electromagnetic applications has considerably grown in the past few years.¹ Commensurately the theory and understanding of wave propagation in metamaterials has progressed at a rapid pace, as exemplified by the many homogenization models recently proposed.^{2–14} The main purpose of all homogenization methods is to properly model the metamaterial response as a bulk material with a limited number of macroscopic parameters. In many ways this homogenization is analogous to the macroscopic electromagnetic modeling of natural materials.^{15,16} Nonetheless, simple quasistatic mixing formulas and homogenization methods for natural materials¹⁷ have inherent limitations when applied to several metamaterial geometries; see, for example, Ref. 18. Improved models are necessary in order to properly represent the physics of these artificial materials, especially in frequency ranges where anomalous frequency and spatial dispersion effects arise that do not usually occur in natural materials. Indeed, despite the progress in metamaterial modeling, there are important features of metamaterials that are not always well-captured by their homogenization models. For example, bulk metamaterial parameters should always obey the passivity and causality conditions established for continuum models of natural materials^{15,16} in the spectral regions where they retain their physical meaning; in particular,

$$\varepsilon''(\omega) \geq 0 \quad (1a)$$

$$\frac{\partial \varepsilon'(\omega)}{\partial \omega} > 0, \quad (1b)$$

where $\varepsilon = \varepsilon' + i\varepsilon''$ is the bulk permittivity and an $e^{-i\omega t}$ time dependence is assumed throughout. The second inequality applies strictly to transparency windows with negligible loss. Similar considerations should in general apply also to the bulk permeability, even though here things may become more subtle, at least in the case of artificial magnetism (that is, magnetism produced by electric-current distributions over finite volumes) and of diamagnetic materials.¹⁹

It is well known that commonly retrieved metamaterial constitutive parameters often violate conditions (1), exhibiting antiresonant artifacts near the metamaterial resonances,^{20,21} that is, resonant dispersion features that violate conditions (1). As discussed in Ref. 18 some of these artifacts can be corrected with improved homogenization models aimed at restoring the local meaning of permittivity and permeability. However, even away from these resonances, and in frequency regions for which simple quasistatic considerations are expected to apply,² homogenization models often show anomalous negative slope-dispersion curves of permittivity and permeability violating condition (1b).

In this context it has been suggested that metamaterial characteristics such as negative or near-zero material parameters and index of refraction violate causality²² and that metamaterials may overcome classic causal limitations such as the velocity with which signals may be transmitted.²³ In contrast we show in this paper that exact metamaterial homogenized parameters must *always* satisfy the same causality constraints at a fixed spatial frequency as do the material parameters that comprise their constituents. However, we will show that causality may be inherently violated in widely used approximate metamaterial homogenization models based on classic Maxwell-Garnett approaches. We prove, in particular, that the point-dipole approximations used in these models inherently introduce noncausal features into the dynamic electromagnetic interaction among the metamaterial inclusions. We determine the cause of this noncausality, and we suggest a method for restoring the proper causal response to bulk metamaterial models, retaining the advantages of point-dipole approximations.

We do not necessarily mean to caution against the use of point-dipole models in the homogenization of metamaterials, which are often useful and accurate. It is, however, very important to recognize the noncausality that is *always* introduced when point-dipole models are used which, as will be shown in the following, can lead to unphysical results in modeling several metamaterial geometries of interest.

It is relevant to point out that Maxwell-Garnett approaches to the homogenization of composites have a long

tradition, which dates back to over a century ago.¹³ Lord Rayleigh himself pointed out²⁴ that quasistatic dipolar approximations cannot accurately describe densely packed arrays, and multipolar approaches have been developed through the years to correct these issues.²⁵ The noncausal features highlighted in this paper, however, are not directly related to these well-understood effects and limitations. Our work focuses on array designs for which the dipolar approximations are usually well justified, and their weight compared to any other multipolar order is significantly larger. We focus on another, more subtle source of inconsistency that directly stems from using Maxwell-Garnett approaches in combination with refined dynamic expressions for the point-dipole model of the inclusions and the array interaction constants. These refined models, which have been put forward specifically for metamaterials to improve the accuracy of Maxwell-Garnett homogenization methods, are shown to inherently introduce noncausal features that should be accurately considered. This inconsistency becomes particularly important when dealing with densely packed arrays of inclusions, typical for metamaterials.

The paper is organized as follows. The central equations of causality, the Kramers-Kronig relations and condition (1b) are derived and applied to metamaterials in Sec. II. In Sec. III we show how the Maxwell-Garnett approach applied to metamaterial arrays can violate the Kramers-Kronig causality relations even in the case of fixed-spatial wave number (i.e., considering possible spatial dispersion effects in the metamaterial). Because the derivation of condition (1b) is based on the assumption that passivity constraints is satisfied, in Sec. IV we prove that the usual Maxwell-Garnett expression for electric susceptibility is strictly consistent with passivity requirements at all frequencies. In Secs. V and VI we enter the core of the paper, investigating the cause of noncausality features and violation of the Kramers-Kronig relations. We begin in Sec. V by exploring the noncausality introduced by concentrating the polarizability of a metamaterial inclusion into a point-dipole at its center. We show that noncausality features are inherently introduced at this stage of homogenization, because the time response of an inclusion of finite size excited by an external field anticipates the radiation from an ideal point-dipole placed at its center, where the inclusion's polarizability is assumed to be concentrated. A generalized form of the Kramers-Kronig relations is derived to take this effect into account. The analysis of the noncausality of the polarizability of a single-isolated sphere carries over immediately to dilute random arrays because for these arrays the interaction constant can be neglected, and hence their susceptibility is proportional to the polarizability of the single inclusion. In Sec. VI these concepts are extended to general metamaterial arrays, showing that their noncausal response, associated with the dipolar approximations, becomes particularly important for densely packed metamaterials, for which the time advance associated with the polarizability response is comparable with the time delay that a signal takes to cross one unit cell. In Sec. VII and in the two Appendices we further discuss the issue of causality and metamaterial homogenization, showing that a rigorous full-wave definition of effective parameters is inherently causal. In Sec. VIII we put forward a method

to modify the Maxwell-Garnett approach in order to restore a causal response, still relying on dipolar approximations. Finally in Sec. IX we present our conclusions.

II. CAUSALITY IN METAMATERIALS

Since causality and the Kramers-Kronig relations for metamaterials play a central role in this paper, they will be derived in this section. Any passive and causal physical system has an impulse response in time, for example the electric susceptibility $\chi_t(t)$, that is zero for any $t < 0$. As a direct consequence¹⁵ its Fourier transform $\chi(\omega)$ is an analytic function of complex ω that has no poles and $\chi(|\omega| \rightarrow \infty) = 0$ for any $\text{Im}[\omega] > 0$. The Kramers-Kronig relations for $\chi(\omega)$ can be then obtained by applying the Cauchy integral formula to a semicircle enclosing the upper half of the complex ω plane¹⁵

$$\chi(\omega) = \frac{-i}{\pi} P \int_{-\infty}^{\infty} \frac{\chi(\Omega)}{\Omega - \omega} d\Omega. \quad (2)$$

A sufficient condition for the integral in Eq. (2) over the real axis to be well-defined for all real ω is that $\chi(\Omega)$ be Hölder-continuous and decay fast enough on the real axis as $|\Omega| \rightarrow \infty$ for the integral to converge.²⁶ The above relation assumes that ω is real-valued. By extracting real and imaginary parts of Eq. (2) for $\chi(\omega) = \chi'(\omega) + i\chi''(\omega)$ and applying the reality condition for the time response $\chi(\omega) = \chi^*(-\omega)$, we obtain¹⁵

$$\chi'(\omega) = \frac{2}{\pi} P \int_0^{\infty} \frac{\Omega \chi''(\Omega)}{\Omega^2 - \omega^2} d\Omega. \quad (3)$$

Similarly it is possible to write $\chi''(\omega)$ as a function of $\chi'(\omega)$. Passivity relations require $\chi''(\Omega) \geq 0$; therefore, taking the derivative of Eq. (3) for frequencies where $\chi''(\Omega)$ is zero (or negligible) yields the condition

$$\frac{\partial \chi'(\omega)}{\partial \omega} = \frac{4\omega}{\pi} \int_0^{\infty} \frac{\Omega \chi''(\Omega)}{(\Omega^2 - \omega^2)^2} d\Omega > 0, \quad (4)$$

which is consistent with condition (1b) since $\varepsilon = \varepsilon_0(1 + \chi)$, where ε_0 is the free-space permittivity. If the bulk permittivity and permeability represent a meaningful physical response over the entire real-frequency axis, they should satisfy Eqs. (1b) and (4) in frequency windows with zero (or negligible) absorption. Related inequalities based on a limited-frequency interval, of specific interest for metamaterials, have been derived in Ref. 28. In addition to being time or frequency dependent, the response of most metamaterials is also spatially dispersive, that is, $\chi(\omega)$ is nonlocal and is also a function of the propagation vector $\boldsymbol{\beta}$ under an $e^{i\boldsymbol{\beta}\cdot\mathbf{r}}$ spatial variation. As widely discussed in the literature,^{15,16,27} for spatially dispersive materials the previous considerations still hold for $\chi(\omega, \boldsymbol{\beta})$, but only for fixed values of $\boldsymbol{\beta}$.²⁹

III. NONCAUSALITY IN MAXWELL-GARNETT MODELS OF METAMATERIALS

The central focus of this paper is the violation of causality in classic metamaterial homogenization models, the causes of this violation, and possible remedies for it. We focus in this section and the rest of the paper on one of the most

used homogenization models, based on the Maxwell-Garnett approach, and we show that this model inherently leads to noncausal features in the bulk response. As mentioned previously, spatial dispersion is often the cause of anomalous response in metamaterials, and it has to be taken into account to rigorously apply Maxwell-Garnett principles. In this regard a generalized Maxwell-Garnett homogenization of periodic arrays of dielectric inclusions, which properly accounts for spatial and frequency dispersion, has been put forward in Ref. 12, showing that it is possible to relate the spatially averaged electric field \mathbf{E}_{av} to the averaged displacement vector \mathbf{D}_{av} by a generalized permittivity dyadic

$$\mathbf{D}_{\text{av}} = \underline{\epsilon}(\omega, \boldsymbol{\beta}) \cdot \mathbf{E}_{\text{av}}, \quad (5)$$

under the assumption of $e^{i(\boldsymbol{\beta} \cdot \mathbf{r} - \omega t)}$ space-time dependence. This single-parameter generalized constitutive relation was originally introduced to describe natural optical crystals.^{15,16} This homogenization approach implicitly combines the electric and magnetic responses of the inclusions into the single effective permittivity dyadic $\underline{\epsilon}(\omega, \boldsymbol{\beta})$. It is shown in Appendix A that the exact expression for $\underline{\epsilon}(\omega, \boldsymbol{\beta})$, as defined in Ref. 12, always satisfies exactly the causality relation Eq. (2) for fixed, arbitrary $\boldsymbol{\beta}$.

An alternative rigorous homogenization approach, using the more traditional bianisotropic effective constitutive dyadics (instead of the single permittivity dyadic) is developed in Ref. 14. With the interaction among the inclusions described by concentrated (point) electric and magnetic dipoles, and approaching the long spatial wavelength limit $\beta = 0$, the magneto-electric coupling is negligible,¹⁴ and both approaches¹²⁻¹⁴ yield a simple generalized form of the Clausius-Mossotti homogenization formulas.¹⁷ In particular the electric susceptibility response for a cubic-lattice array is given by

$$\chi_{\text{eff}}(\omega) = \frac{1}{d^3(\alpha_e^{-1} - C_{\text{int}})}, \quad (6)$$

where d is the array period, α_e is the electric polarizability of the inclusions in each unit cell, defined such that the induced dipole moment is given by $\mathbf{p} = \varepsilon_0 \alpha_e \mathbf{E}_{\text{loc}}^0$, and $\mathbf{E}_{\text{loc}}^0$ is the electric field at the center of the particle. By its same definition, the electric polarizability is directly proportional to the first-order transverse-magnetic (TM) Mie-scattering coefficient, describing the scattering from the isolated inclusion.³⁰ The interaction constant C_{int} describes the full-wave electric-electric dynamic coupling among the inclusions for a transverse electromagnetic wave with respect to one of the principal directions of the cubic array.¹⁴ The expression (6), which will be rigorously derived using a Maxwell-Garnett homogenization approach in Sec. VII, represents the dynamic electric response of the metamaterial under the previous assumptions, and it is consistent with the homogenization approaches used in Refs. 7,8,10, and 14. An analogous formula can be derived for the magnetic susceptibility as a function of the magnetic polarizability α_m . In the quasistatic limit $C_{\text{int}} \simeq 1/(3d^3)$, and Eq. (6) reduces to the usual Clausius-Mossotti homogenization formula commonly used in quasistatic-metamaterial models.¹⁷ This confirms that in the static regime all these homogenization approaches correctly converge to the classic continuum model.

Quasistatic approaches neglect the inherent frequency dependence attributable to the finite velocity of wave propagation and therefore avoid noncausality problems. When more refined dynamic models such as the one in Eq. (6) are considered, even for a fixed value of $\boldsymbol{\beta}$, it is common to encounter significant violations of the causality condition (1b), which imply that the Kramers-Kronig relations for passive media do not hold. This issue is evident in numerical examples presented in recent papers^{10,14} with models consistent with Eq. (6) using rigorous dynamic expressions for C_{int} and displaying negative-slope frequency dispersion curves for $\epsilon'(\omega)$, even where $\beta d \simeq \omega d/c \simeq 0$ and the absorption is zero.

To demonstrate the noncausality associated with Eq. (6), we consider here the simplest possible example of a metamaterial homogenization problem: an array with zero phase-shift across each unit cell ($\beta d = 0$). Under this assumption the effective electric susceptibility given by Eq. (6) is expected to represent a very good approximation for the dielectric metamaterial response. It is straightforward to demonstrate, however, that the dynamic expression in Eq. (6) can violate condition (1b) and thus the Kramers-Kronig relations for passive media, even in the ideal case for which βd is kept constant and identically equal to zero. To see this, consider a metamaterial array comprised of lossless dielectric spheres of radius a with permittivity $\varepsilon > \varepsilon_0$ and permeability μ_0 . The exact dynamic polarizability of each sphere can be obtained directly from Mie scattering theory³⁰:

$$\alpha_d(\omega) = \frac{6\pi}{k_0^3} \left(\frac{v}{u} - i \right)^{-1} \quad (7)$$

with

$$u = \begin{vmatrix} j_1(ka) & j_1(k_0a) \\ [(ka)j_1(ka)]'/\varepsilon & [(k_0a)j_1(k_0a)]'/\varepsilon_0 \end{vmatrix},$$

$$v = \begin{vmatrix} j_1(ka) & y_1(k_0a) \\ [(ka)j_1(ka)]'/\varepsilon & [(k_0a)y_1(k_0a)]'/\varepsilon_0 \end{vmatrix}.$$

The wave number in the sphere is $k = k_0 \sqrt{\varepsilon/\varepsilon_0}$, and $k_0 = \omega/c$ is the free-space wave number. The exact dynamic expression for the interaction constant C_{int} , which we give in Sec. VII, has been obtained and used in several recent papers on generalized Maxwell-Garnett homogenization principles.^{7,8,10,12,14}

Since we are interested in the long-wavelength regime for which homogenization principles are applicable ($k_0 d \ll 2\pi, \beta d \ll 2\pi$), to demonstrate the noncausality it is sufficient to consider the second-order Taylor expansion of the terms in Eq. (6) with respect to k_0 . Specifically, for $\beta d = 0$ the interaction constant in a cubic lattice is approximated by the first three terms of its power series¹²:

$$C_{\text{int}} \simeq d^{-3} \left[\frac{1}{3} - 0.1505(k_0 d)^2 - i \frac{(k_0 d)^3}{6\pi} \right]. \quad (8)$$

Similarly, the inverse polarizability in Eq. (7) becomes

$$\alpha_d^{-1} \simeq a^{-3} \left[\frac{1}{4\pi} \frac{\varepsilon + 2\varepsilon_0}{\varepsilon - \varepsilon_0} - \frac{3(k_0 a)^2}{20\pi} \frac{\varepsilon - 2\varepsilon_0}{\varepsilon - \varepsilon_0} - i \frac{(k_0 a)^3}{6\pi} \right]. \quad (9)$$

Combining these two expressions recasts Eq. (6) in the form

$$\chi_{\text{eff}}(k_0d \rightarrow 0, \beta d = 0) = \frac{\chi_{\text{eff}}(0)}{1 - \chi_{\text{eff}}(0) \left[\frac{3(\varepsilon - 2\varepsilon_0)d}{20\pi(\varepsilon - \varepsilon_0)a} - 0.1505 \right] (k_0d)^2}, \quad (10)$$

where the static expression of the electric susceptibility is given by¹⁷

$$\chi_{\text{eff}}(0) = \left(\frac{(d/a)^3 \varepsilon + 2\varepsilon_0}{4\pi \varepsilon - \varepsilon_0} - \frac{1}{3} \right)^{-1}. \quad (11)$$

It is evident that the slope of $\chi_{\text{eff}}(\omega)$ versus frequency for small k_0d is determined by the coefficient of $(k_0d)^2$ in the denominator of Eq. (10) and that, for sufficiently densely packed arrays (smaller d/a), the effective susceptibility obtained with a full wave point-dipole dynamic model inherently violates condition (1b), that is, produces a negative slope in $\chi_{\text{eff}}(\omega)$. In fact it is simple to show that a positive slope for $\chi_{\text{eff}}(k_0d \rightarrow 0^+, \beta d = 0)$ may be obtained *if and only if* the following conditions are simultaneously satisfied:

$$\begin{cases} \varepsilon > 2\varepsilon_0 \\ \frac{d}{a} > \pi \frac{\varepsilon - \varepsilon_0}{\varepsilon - 2\varepsilon_0} \end{cases}. \quad (12)$$

The inequalities (12) imply that inclusions that are too densely packed or have too low a permittivity produce a negative slope in the effective metamaterial permittivity and thereby do not satisfy the Kramers-Kronig causality relations for passive media. In Sec. V we show that dilute metamaterial arrays homogenized according to Eq. (6) inherently violate causality, and we show the reason for this violation. Surprisingly we find in Sec. VI that the Kramers-Kronig relations can *never* be satisfied by Eq. (6), independent of the array density and material permittivity, even for design parameters that satisfy Eqs. (12). In fact it is possible to have a positive slope and yet violate the Kramers-Kronig relations, as will be shown in Sec. VI. In other words the Kramers-Kronig causality relations are sufficient but not necessary to ensure the positive slope of the susceptibility.

In usual composites and mixtures these noncausal features are hardly noticeable because the noncausal time advance introduced by the point-dipole approximation is much smaller than the time the signal takes to cross one array period. This is translated into a positive slope of $\chi_{\text{eff}}(\omega)$, as conditions (12) are typically satisfied. In contrast for metamaterials and for densely packed arrays these artifacts may become very important, as we describe in the following.

For this reason we derive a generalized form of the Kramers-Kronig relations that compensates for the noncausality introduced by the point-dipole approximation, and we discuss the conditions under which $\chi_{\text{eff}}(\omega)$ may regain its causal response. Finally we show how to correct the noncausality when the inequalities (12) are not satisfied, still retaining the advantages of a dipolar homogenization model. Our results can be generalized to inclusions other than spheres and to nonzero fixed values of β by applying similar procedures.

IV. PASSIVITY

Before discussing causality further, it is important to establish that the dynamic expression (6) *always* satisfies the

passivity condition (1a) for any real ω because the derivation of condition (1b) relies on the array passivity [see Eq. (4)]. Any passive particle is characterized by a polarizability function satisfying³¹

$$\alpha_e^{-1}(\omega) = \text{Re}[\alpha_e^{-1}] - i \frac{k_0^3}{6\pi} - i\alpha_{\text{loss}}^{-1}, \quad (13)$$

where its imaginary part is derived from power conservation, the first imaginary term accounting for dipolar radiation loss³¹ and the second imaginary term accounting for absorption loss with $\alpha_{\text{loss}}^{-1} \geq 0$. The interaction constant C_{int} has an imaginary part that exactly compensates for the radiation loss in Eq. (13), that is, $\text{Im}[C_{\text{int}}] = \frac{k_0^3}{6\pi}$, independent of d .^{7,12} This implies that Eq. (6) can be rewritten as

$$\chi_{\text{eff}}(\omega) = \frac{1}{d^3 (\text{Re}[\alpha_e^{-1}] - \text{Re}[C_{\text{int}}] - i\alpha_{\text{loss}}^{-1})}, \quad (14)$$

which ensures that $\text{Im}[\chi_{\text{eff}}(\omega)] \geq 0$, with the equal sign holding for lossless inclusions. This result confirms that the function $\chi_{\text{eff}}(\omega)$ satisfies the passivity condition (1a) for any periodic array, independent of the nature of the inclusion and its period.

V. NONCAUSALITY OF THE POLARIZABILITY FUNCTION AND DILUTE METAMATERIAL ARRAYS

In this section we begin to investigate why the effective susceptibility given by Eq. (6) violates the causality conditions. To determine the cause of its noncausality, we analyze the individual elements of Eq. (6), starting in this section with the polarizability response of a single dielectric sphere $\alpha_e(\omega)$. It is important to note that, in the limit of dilute random (nonperiodic) arrays of particles, $\chi_{\text{eff}}(\omega) \simeq \alpha_e(\omega)/d^{3,17}$ where d is now the average distance between the inclusions. Hence, the following analysis of the polarizability of an isolated sphere carries over immediately to the susceptibility of a dilute random array.

We use and compare the exact dynamic expression for the polarizability of a dielectric sphere $\alpha_d(\omega)$, as given by Eq. (7), and its quasistatic expression with the proper radiation-loss correction

$$\alpha_s(\omega) = \frac{6\pi}{k_0^3} [(k_0a x)^{-3} - i]^{-1}, \quad (15)$$

where $x = \sqrt{\frac{2}{3} \frac{\varepsilon - \varepsilon_0}{\varepsilon + 2\varepsilon_0}}$. Eq. (15) is obtained from $\alpha_d(\omega)$ in Eq. (7) by taking the limit as $(k_0a) \rightarrow 0$ but keeping the imaginary term in the square brackets to ensure that the passivity condition is satisfied as a consequence of the unavoidable radiation loss. Eq. (15) is a good approximation to Eq. (7) for long free-space wavelengths.

In Fig. 1 we show the calculated polarizability spectra for two typical examples of interest: $\varepsilon = 3\varepsilon_0$ [Fig. 1(a)] and $\varepsilon = 20\varepsilon_0$ [Fig. 1(b)]. The figures show real and imaginary parts of the normalized polarizability (top and bottom rows, respectively) and the comparison between α_s (solid blue lines) and α_d (solid red lines). The polarizability spectrum is mainly concentrated in the region $k_0a < 4$, beyond which higher-order multipoles dominate the scattering. This is the most interesting frequency range for homogenization purposes

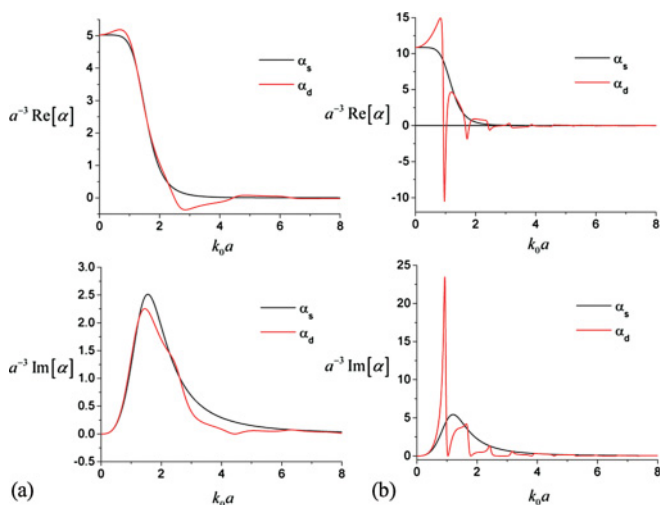


FIG. 1. (Color online) Normalized polarizability spectrum for a sphere of radius a and permittivity: (a) $\varepsilon = 3\varepsilon_0$, (b) $\varepsilon = 20\varepsilon_0$ versus frequency.

because the metamaterial inclusions are smaller in size than the wavelength. The quasistatic approximation is accurate for lower permittivity spheres that do not support strong resonances in this frequency range. As expected, the quasistatic approximation cannot represent the dynamic resonances of the higher permittivity spheres that produce sharp peaks in the dynamic polarizability of Fig. 1(b). Both expressions satisfy the passivity requirement $\text{Im}[\alpha_e] \geq 0 \forall \omega$ as expected.

Surprisingly, however, it is shown next that neither the dynamic susceptibility expression, Eq. (7), nor the quasistatic susceptibility expression, Eq. (15), satisfy the Kramers-Kronig relations (2), that is, they do not provide a causal scattering response in time. This was noticed as an aside in Ref. 32, but it has not been pursued in the literature to the best of our knowledge. To prove this, we calculate the inverse Fourier transform of Eq. (15), which for any $\varepsilon > \varepsilon_0$ is given by

$$\alpha_{\text{st}}(t) = 2\pi c a^2 x^2 \left[e^{\frac{ct}{xa}} u(-t) + e^{-\frac{ct}{2xa}} \times \left(\cos \frac{\sqrt{3}ct}{2xa} + \sqrt{3} \sin \frac{\sqrt{3}ct}{2xa} \right) u(t) \right], \quad (16)$$

where $u(t)$ is the Heaviside-step function. It is evident that the time response of the quasistatic polarizability is nonzero for $t \leq 0$. In particular it has the finite value

$$\alpha_{\text{st}}(0) = 2\pi c x^2 a^2 \quad (17)$$

at time $t = 0$ and an anticausal exponential advance with time constant xa/c for $t < 0$. In Fig. 2 we plot the calculated time response for the two numerical examples of Fig. 1, comparing the analytical result (16) for the quasistatic polarizability (solid blue lines) with the numerically calculated inverse Fourier transform of α_d (solid red lines). The curves in Fig. 2 are normalized to the value $\alpha_{\text{st}}(0)$ in each plot. The time response of the quasistatic polarizability closely follows the dynamic (exact) response in the transient regime [small values of $|ct/(2a)|$], but it fails to agree well, as expected, with the later dynamic response in the presence of the strong resonances that exist for larger permittivity [Fig. 2(b)]. The anticausal advance

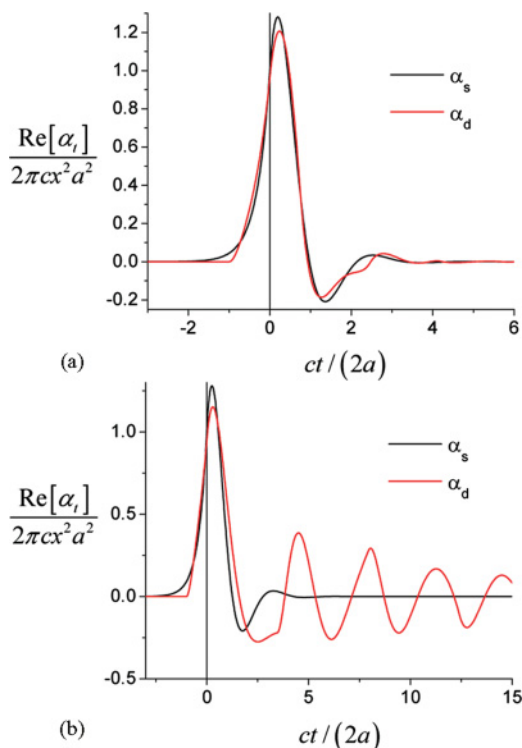


FIG. 2. (Color online) Time response for the polarizability spectra of Fig. 1: a sphere of radius a and permittivity (a) $\varepsilon = 3\varepsilon_0$, (b) $\varepsilon = 20\varepsilon_0$.

for $t < 0$, of most interest for the present analysis, agrees well with the exponential advance in Eq. (16).

There is, however, a feature of the dynamic polarizability expression that differs from the quasistatic expression: its time response is identically zero for any $t < -2a/c$. In other words the dynamic polarizability time response is noncausal, but its anticausal advance begins exactly at $t = -2a/c$ for any value of ε . This feature provides the clue for understanding the noncausal behavior of the polarizability: since α_d represents the scattering amplitude of the first TM spherical harmonic (electric-dipole moment) scattered by a sphere of finite radius a , it is evident that, although the dipole moment is evaluated at the center of the sphere, and by definition the instant $t = 0$ corresponds to the moment in which the impinging excitation hits this center point, the sphere interaction with the excitation field actually starts when the impinging wave hits its surface, that is, at time $t = -a/c$. Moreover, the scattered radiation has a time advance of another $t = -a/c$, since it first originates from the surface of the sphere, rather than from the $t = 0$ reference point at its center. The total time advance compared to an ideal dipole radiating at the origin is exactly $t = -2a/c$ (provided that the sphere material is causal), which is indeed the exact instant at which the transient response of α_d starts in both examples of Fig. 2. The quasistatic approximation (16) cannot perfectly represent this noncausal response, but it approximates it well with an anticausal exponential advance. These considerations imply that the time response $\alpha_{\text{dt}}(t)$, that is, the inverse-Fourier transform of $\alpha_d(\omega)$, must satisfy the generalized causality equation

$$\alpha_{\text{dt}}(t) = \alpha_{\text{dt}}(t)u(t + 2a/c). \quad (18)$$

This finding clearly explains why the frequency curves in Fig. 1 cannot satisfy the Kramers-Kronig's relations: Eq. (18) ensures that the function $\alpha_d(\omega)e^{i\omega 2a/c}$ is strictly causal and therefore $\alpha_d(\omega)$ cannot have poles in the upper complex half plane. However, the contribution from the large semicircle $|\omega| \rightarrow \infty$ in Cauchy's integral is not necessarily zero, since Eq. (18) does not ensure that $\alpha_d(|\omega| \rightarrow \infty)$ converges to zero. It may be indeed proven using Eq. (7) that

$$\lim_{|\omega| \rightarrow \infty} \alpha_d(\omega) = \frac{3c^3\pi}{\omega^3} \left[i + e^{-i\omega \frac{2a}{c}} \left(\frac{2}{\sqrt{\epsilon} \cot\left[\frac{ka}{c}\right]} - i \right) \right], \quad (19)$$

which goes to zero only after $\alpha_d(\omega)$ is multiplied by an exponential $e^{i\omega\delta}$ with $\delta \geq 2a/c$, consistent with Eq. (18) and with our physical intuition. We can therefore write a generalized form of the Kramers-Kronig relation (3) using Eq. (18):

$$\alpha'_d(\omega) = \frac{2}{\pi} P \int_0^\infty \frac{\Omega \alpha''_d(\Omega)}{\Omega^2 - \omega^2} d\Omega + 2 \int_{-2a/c}^0 \alpha_{dt}(t) \cos(\omega t) dt. \quad (20)$$

This equation shows that the real part of the dynamic polarizability may be related to the sum of the usual causal-relation integral over the imaginary part, plus an additional contribution stemming from the point-dipole approximation for a scatterer of finite size, which consists of the noncausal contribution to the Cauchy's integral formula stemming from the nonzero contribution at $|\omega| \rightarrow \infty$. This correction becomes negligible as the radius of the scatterer decreases in value ($a \rightarrow 0$), as expected.

For the quasistatic polarizability, we can evaluate in closed form the second (noncausal) term on the right-hand side of Eq. (20), to obtain

$$\alpha'_s(\omega) = \frac{2}{\pi} P \int_0^\infty \frac{\Omega \alpha''_s(\Omega)}{\Omega^2 - \omega^2} d\Omega + \frac{4\pi c^2 x^3 a^3}{c^2 + x^2 a^2 \omega^2}, \quad (21)$$

in which the second term on the right-hand side provides a very good approximation to the dynamic noncausal transient correction in Eq. (20).

It is evident from the time-domain response that the analytical properties of $\alpha_s(\omega)$ provide clear insights into the noncausal response of α_d , since it is strictly concentrated in the transient regime. Without the correction term for point-dipolar radiation required by passivity, the quasistatic polarizability expression (15) would neglect frequency dispersion and it would yield the constant value $6\pi a^3 x^3$ for any frequency ω . This corresponds to a (causal) Dirac $\delta(t)$ response in the time domain. Adding the required imaginary unit in Eq. (15) introduces poles into the expression for $\alpha_s(\omega)$, which are evident after writing explicitly its real and imaginary parts:

$$\alpha'_s(\omega) = \frac{6\pi c^6 x^3 a^3}{c^6 + x^6 a^6 \omega^6} \quad (22a)$$

$$\alpha''_s(\omega) = \frac{6\pi \omega^3 c^3 x^6 a^6}{c^6 + x^6 a^6 \omega^6}. \quad (22b)$$

As an aside, it may be verified that these expressions do exactly satisfy Eq. (21).

The point-dipole radiation correction adds three pairs of complex conjugate poles in Eq. (21), with three of the poles in the upper half complex ω plane. Of these only the purely imaginary pole $\omega_1 = i\sqrt{ca/x}$ has a nonzero residue $-2i\pi cx^2 a^2$ whose amplitude is identical to the value of $\alpha_{st}(0)$ in Eq. (17). Indeed, the correction term

$$\alpha'_{nc} = \frac{4\pi c^2 x^3 a^3}{c^2 + x^2 a^2 \omega^2} = \text{Re} \left[\frac{2i\pi cx^2 a^2}{\omega_1 - \omega} \right] \quad (23)$$

on the right-hand side of Eq. (21), associated with the noncausal response of α_{st} , provides an anti-Lorentzian response with complex conjugate poles at $\omega = \pm i\sqrt{ca/x}$, precisely associated with this residue term.³³ Applying the Cauchy integral formula to the large semicircle around the upper-half complex plane and taking into account the residue at $\omega = i\sqrt{ca/x}$, it is indeed possible to obtain the same relation Eq. (21), as shown in the last identity in Eq. (23). It is not surprising to realize that the presence of noncausal poles in the upper-half complex plane stems from the point-dipole radiation correction to the quasistatic polarizability expression, since we have noticed that this noncausality is physically associated with the re-radiation and scattering from a sphere of finite size.

In its full dynamic expression, the noncausal response of $\alpha_d(\omega)$ in the right-hand side of Eq. (20) is well approximated by the quasistatic closed-form noncausal contribution (23). The generalized Kramers-Kronig relation for the dynamic polarizability Eq. (20) may therefore be approximated in closed form as

$$\alpha'_d(\omega) \simeq \frac{2}{\pi} P \int_0^\infty \frac{\Omega \alpha''_d(\Omega)}{\Omega^2 - \omega^2} d\Omega + \frac{4\pi x^3 a^3}{1 + (xk_0 a)^2}. \quad (24)$$

Figure 3 shows the comparisons between (a) the exact expression for $\alpha'_d(\omega)$ (as in Fig. 1), (b) the value that one would obtain from $\alpha''_d(\omega)$ by simply using the Kramers-Kronig relations [effectively from Eq. (3) or Eq. (20) without the correction attributable to noncausality], and (c) the approximate value obtained using Eq. (24) for the two examples of Fig. 1. The usual Kramers-Kronig relations are unable to relate real and imaginary parts of the dynamic polarizability because of its inherently noncausal response corrected by Eq. (24). The required additional contribution stemming from the nonzero value of Eq. (19) is well approximated by its quasistatic closed-form expression (23), used in Eq. (24). This is consistent with the transient response of the dynamic polarizability being well approximated by its quasistatic response. The dynamic resonances in the larger permittivity example are all associated with causal poles, placed in the lower-half complex plane outside the Cauchy integration path, and therefore they are correctly captured by the integral in Eq. (21). The quasistatic term added in Eq. (24) effectively takes into account the transient anticausal response associated with the approximation of concentrating the polarization response of a sphere of finite radius into one point, and it shows that its contribution to the Cauchy integral formula, represented by the nonzero value of $\alpha_d(\omega)$ for $|\omega| \rightarrow \infty$ in Eq. (19), may be well approximated by a single pole on the imaginary axis in the upper-half complex plane.

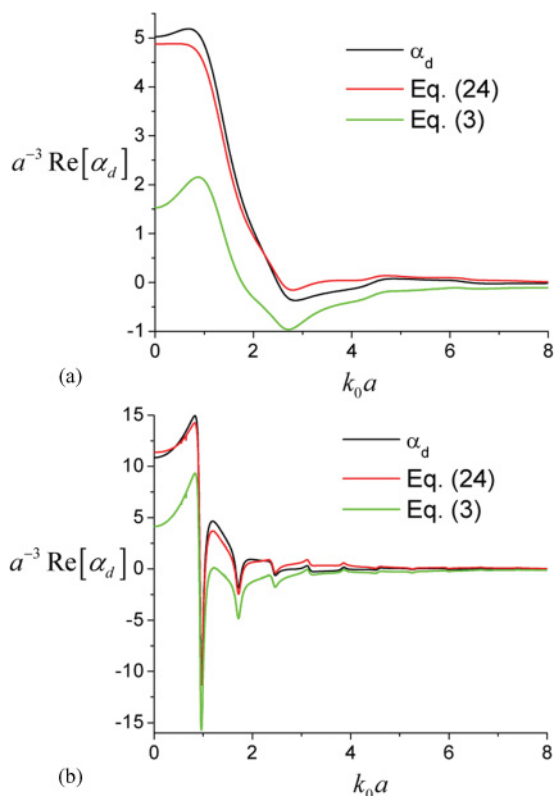


FIG. 3. (Color online) Comparisons among the exact value of $\alpha'_d(\omega)$, the value calculated using $\alpha'_d(\omega)$ in the standard Kramers-Kronig relation (3), and the value obtained using the generalized formula (24). Panels (a) and (b) refer to the examples in Fig. 1.

To summarize, we have shown so far in this section that the polarizability response of an isolated sphere of finite radius a is inherently noncausal because of having approximated the scattering from a finite-diameter sphere by the radiation from a single-point dipole at its center. A fully causal scattering response may be obtained only after considering the exact boundary conditions on the surface of the sphere. In particular, higher-order multipolar terms, usually considered negligible in the frequency range of interest for typical homogenization problems ($k_0 a < 1$), become necessary to rigorously model the causality of the scattering response of a finite size object. Translated to the homogenization problem, this concept is verified in Appendix A, where it is rigorously proven that a full-wave derivation, without making use of point-dipole approximations, of the homogenized dielectric response of any metamaterial array for a fixed β necessarily yields a causal effective permittivity.

As pointed out previously, analogous considerations apply to dilute arrays of randomly positioned inclusions for which the effective permittivity obtained within the point-dipole approximation will exhibit similar noncausality, since for these arrays the interaction constant can be neglected, and hence $\chi_{\text{eff}}(\omega)$ is simply proportional to $\alpha_e(\omega)$. In such arrays the generalized Kramers-Kronig relation (24) yields for the susceptibility

$$\chi'_{\text{eff}}(\omega) \simeq \frac{2}{\pi} P \int_0^\infty \frac{\Omega \chi''_{\text{eff}}(\Omega)}{\Omega^2 - \omega^2} d\Omega + \frac{4\pi x^3 \gamma^{-3}}{1 + (xk_0 a)^2}, \quad (25)$$

where $\gamma = d/a$ represents the density factor of the array. By taking the derivative of Eq. (25) in transparency regions and using $\epsilon_{\text{eff}} = \epsilon_0(1 + \chi_{\text{eff}})$, we obtain

$$\frac{\partial[\epsilon'_{\text{eff}}(\omega)]}{\partial\omega} \simeq \frac{4\omega}{\pi} \int_0^\infty \frac{\Omega \epsilon''_{\text{eff}}(\Omega)}{(\Omega^2 - \omega^2)^2} d\Omega - \frac{8\pi \epsilon_0 x^3 \gamma^{-3} (xk_0 a)^2}{\omega [1 + (xk_0 a)^2]^2}, \quad (26)$$

which generalizes Eq. (4) to the case of random dilute metamaterial arrays.

Equation (26) shows that the noncausal polarizability response adds a negative contribution to the derivative of $\epsilon'_{\text{eff}}(\omega)$. In the case of more densely packed arrays (smaller γ), this negative term may dominate the right-hand side of Eq. (26), possibly leading to anomalous (negative-slope) dispersion of the effective permittivity. This effect is quite simple to understand from a physical point of view, since we have determined that the polarizability response anticipates the excitation by a time interval $2a/c$. If the density of the array is too large, this time interval becomes comparable to the time that the excitation advance takes to travel across the average period along the array, and the small time advance introduced by the point-dipole approximation becomes relevant in the array homogenization, reflected in the negative slope of $\epsilon'_{\text{eff}}(\omega)$. In contrast if the array is very sparse, as in the case of natural materials and mixtures, the small time advance associated with the finite size of the inclusions is negligible compared to the average period in the array, and classic Maxwell-Garnett approaches are well suited for homogenization purposes.¹⁷ This discussion agrees with the general conditions (12), which indeed predict that a negative derivative in the effective permittivity and anomalous negative-slope dispersion arise for more densely packed metamaterial arrays, even after relaxing the assumption of a dilute random array that we have made to derive Eq. (26).

It is relevant to point out that we have also analyzed in detail the case of *periodic* dilute arrays (not reported here for sake of brevity), for which the point-dipole radiation correction in the polarizability is cancelled by the array periodicity. These dilute periodic arrays are of particular interest because we have shown previously in this section, preceding Eq. (22), that the radiation correction is directly associated with the appearance of complex conjugate poles in α_s and with its noncausal response. We have verified, however, that even for periodic dilute arrays, an anticausal response with similar time advance is obtained in the fully dynamic case, and a negative slope of $\chi'_{\text{eff}}(\omega)$ may be produced, especially for smaller values of ϵ/ϵ_0 .

VI. CAUSALITY IN ARBITRARILY DENSE METAMATERIALS

In the previous section we considered dilute random arrays for which the interaction constant C_{int} can be neglected in the expression (6) for the effective susceptibility. We showed that there is then an inherent noncausality in the susceptibility caused by the concentration of the unit-cell polarization in a point-dipole at its center. In this section we continue this investigation by considering arbitrarily dense metamaterial

arrays. For densely packed arrays, as in metamaterials, the influence of C_{int} cannot be neglected, and we analyze here its effects on the causality properties and time response of Eq. (6). In this effort we proceed to study the general causality properties of C_{int} and relate them to the possible misbehavior in the upper half of the complex ω plane.

Using the approximate expressions (8) and (9) for C_{int} and for the inverse polarizability α_d^{-1} , it is simple to prove that χ_{eff} in Eq. (6) has two complex poles for small k_0d at

$$k_0d \simeq \pm \sqrt{\frac{5}{3} \frac{4\pi(\varepsilon - \varepsilon_0) - 3\gamma^3(\varepsilon + 2\varepsilon_0)}{3\pi(\varepsilon - \varepsilon_0) - 3\gamma(\varepsilon - 2\varepsilon_0)}}. \quad (27)$$

Not surprisingly these poles coincide with those in Eq. (10) and are real if and only if conditions (12) are satisfied, implying that too densely packed arrays or too low a permittivity produce the appearance of an anticausal imaginary pole in the upper half of the complex ω plane, reflected in the negative slope of $\chi_{\text{eff}}(\omega)$. The appearance of this pole is qualitatively consistent with the noncausal imaginary pole in $\alpha_s(\omega)$, but its position is now influenced by the array-interaction factor C_{int} . Consistent with the discussions in the previous section, the possible occurrence of this noncausal pole is associated with the use of the point-dipole approximations in obtaining Eq. (6), and it produces a negative slope in $\chi_{\text{eff}}(\omega)$ even in the long-wavelength regime (that is, at frequencies lower than any dynamic resonance of the array), as explained in the previous section. The array-interaction constant C_{int} , representing the array coupling, influences the position of the pole, in agreement with Eq. (27), effectively determining the slope of the effective susceptibility as a function of the array density. In particular the conditions (12) imply, as we have discussed in the context of Eq. (26) for random arrays, that a smaller ratio d/a produces an imaginary (noncausal) pole and the corresponding negative slope in the permittivity dispersion curve in the long-wavelength limit ($k_0d \simeq 0$) when using a generalized Clausius-Mossotti homogenization approach based on point-dipole models. Equations (12) give the necessary and sufficient conditions to avoid a negative slope in the effective permittivity dispersion curve and the presence of an imaginary pole in the upper-half complex plane under the point-dipole approximation for the array interaction. It should be noted, however, that avoiding the negative slope does not ensure a causal behavior, consistent with the discussion following Eqs. (12). As shown in the previous section in connection with Eq. (26), even for less densely packed arrays and positive slopes where conditions (12) are satisfied, we cannot expect that Eq. (6) perfectly obeys the Kramers-Kronig causality relations because the point-dipole approximation inherently introduces a noncausal time response.

In order to confirm these theoretical results, we show in Figs. 4 and 5 the frequency and time response of metamaterial periodic arrays made of spheres similar to those considered in the previous section (see Fig. 2). Since here we consider periodic arrays, we need to add small losses in the spheres to ensure that the time response is finite and bounded (no poles on the real axis in the frequency response). Figure 4 shows the real part of the effective permittivity [calculated using Eq. (6)] for a metamaterial array composed of spheres with $\varepsilon =$

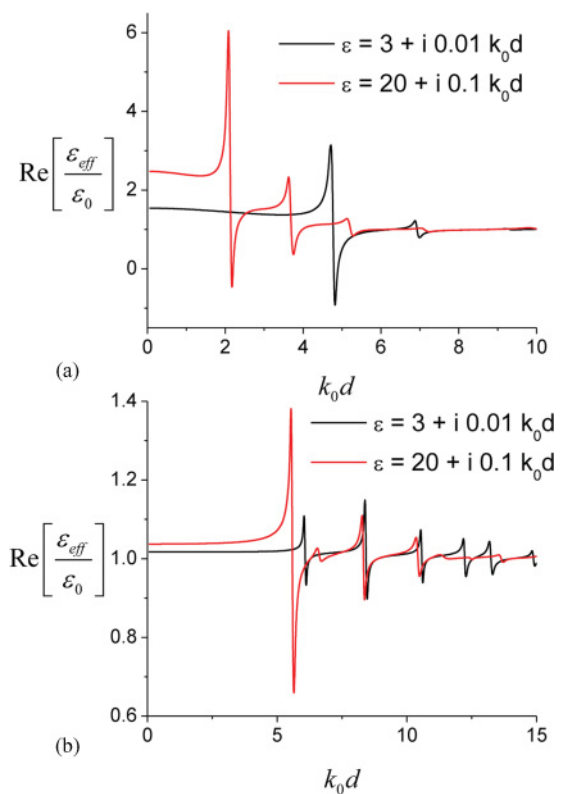


FIG. 4. (Color online) Real part of the effective permittivity, calculated using Eq. (6), for periodic arrays of spheres with $\varepsilon = (3 + i 0.01k_0d)\varepsilon_0$ (black lines) and $\varepsilon = (20 + i 0.1k_0d)\varepsilon_0$ (red lines) and (a) $\gamma = 2.22$, (b) $\gamma = 6.67$.

$(3 + i 0.01k_0d)\varepsilon_0$ (black lines) and $\varepsilon = (20 + i 0.1k_0d)\varepsilon_0$ (red lines).³⁴ Panel (a) shows the results for a very densely packed array $\gamma = 2.22$ and panel (b) for a less densely packed array $\gamma = 6.67$. As expected, the denser array produces a stronger permittivity response and, consistent with Eq. (12), displays anomalous negative-slope dispersion in the long-wavelength regime $k_0d \simeq 0$. A larger permittivity value of the spheres shifts the dynamic (causal) resonances to lower values of k_0d , but it still shows the anomalous negative-slope dispersion in the more densely packed example. In the less densely packed array the frequency response has a positive-slope dispersion curve, but, as we have discussed, this does not mean that the corresponding time response is causal. Figure 5 shows the corresponding time response, obtained from the inverse-Fourier transform of the effective susceptibility Eq. (6). The curves are all normalized to the same arbitrary value for the sake of comparison. As expected, all time responses are decidedly noncausal, and they start at about the same time instant $t \simeq -2a/c$. It is remarkable that the noncausality associated with the point-dipole approximation of the single inclusion dominates the noncausal response for the whole array, whereas C_{int} has only a minor effect on the amount of noncausality in the time response. The more densely packed array with larger permittivity spheres has a time response slightly more noncausal, but in all examples the time advance is dominated by the inherent noncausality of the individual Mie-polarizability response. The causal portion of the time

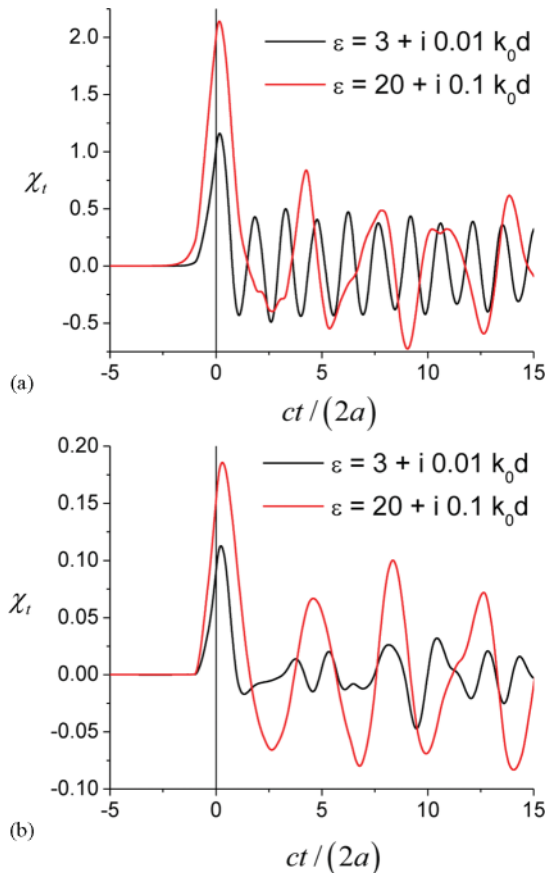


FIG. 5. (Color online) Normalized time response (arbitrary units) for the arrays of Fig. 4, composed by spheres with $\varepsilon = (3 + i 0.01k_0d)\varepsilon_0$ (black lines) and $\varepsilon = (20 + i 0.1k_0d)\varepsilon_0$ (red) and (a) $\gamma = 2.22$, (b) $\gamma = 6.67$. All values are normalized to the same arbitrary units for the sake of comparison.

response reflects the Lorentzian resonances of the arrays, consistent with the curves in Fig. 4.

It is emphasized that, despite all time responses having roughly the same amount of time advance and noncausality features, the effect on the frequency dispersion curve of permittivity strongly depends on the size of the unit cell. For more densely packed arrays the time advance $\sim 2a/c$ is on the same order as the time delay across one unit cell $\sim d/c$, becoming non-negligible in the array homogenization and producing strong anomalous dispersion that violates Eq. (1b). For sparser arrays, satisfying conditions (12), on the other hand, as well as for natural materials and mixtures, this same time advance is less important, since it represents only a minor correction over the typical time delay that the wave takes to cross one unit cell, and the slope of the permittivity dispersion curve remains positive. This is why the concepts introduced here have no drastic effects on the frequency response of Maxwell-Garnett homogenization models for natural materials and composites, but become very important in the proper homogenization of metamaterials.

Sphere permittivities in the range $\varepsilon_0 < \varepsilon < 2\varepsilon_0$ form a peculiar class of metamaterial arrays. Independent of the array density, the conditions (12) are not satisfied, and the array response has noncausal poles in the upper half of the complex

ω plane. This is especially puzzling, since it implies that, even for very small ratios a/d , for which one would expect the point-dipole approximation to hold extremely well in the long-wavelength regime ($k_0d \simeq 0$), such arrays would display anomalous negative-slope frequency dispersion. We have verified this prediction in a series of numerical simulations (not shown here for the sake of brevity). The reason for this unexpected negative slope lies in the fact that the point-dipole approximation always introduces a small advance that is not compensated by the dynamic response of the spheres, because the contrast between the spheres and the background is too small to override the point-dipole approximation for $\varepsilon_0 < \varepsilon < 2\varepsilon_0$. From the viewpoint of Eqs. (9) and (10) the ω^2 Lorentzian term changes sign for $\varepsilon_0 < \varepsilon < 2\varepsilon_0$, and therefore it becomes manifestly noncausal. Of course these low-permittivity spheres are not particularly interesting for most practical purposes, because in the frequency range for which the point-dipole approximation is applicable, arrays with such low-permittivity inclusions are characterized by an extremely weak dielectric response (relative effective permittivity very close to unity).

To conclude we have shown in this section that, even after considering the full dynamic coupling within periodic arrays of inclusions, the dipolar approximations typical of Maxwell-Garnett approaches introduce a noncausal time advance in the same order as the one associated with the polarizability of the individual unit cell, which amounts to $\sim 2a/c$ for spheres of radius a . The array interaction, represented by C_{int} in Eq. (6), has only a minor effect on the amount of time advance in the array response, but it has a significant effect in determining the position of the associated noncausal pole along the imaginary axis of the upper half complex ω plane, associated with the negative slope of the permittivity function for densely packed arrays. In particular when the period d is comparable with the size of the inclusions, the noncausal time advance is reflected in the appearance of an imaginary pole in the upper complex half ω plane and the corresponding violation of condition (1b). In the following sections we further discuss the roots of these noncausal features, and we put forward a method to restore the causality of Maxwell-Garnett homogenization approaches.

VII. FURTHER THOUGHTS ON THE ROOTS OF NONCAUSALITY IN METAMATERIAL HOMOGENIZATION

We have shown in the previous sections how, even after considering the fully dynamic expression for the effective permittivity of a metamaterial array composed of polarizable inclusions, and in the simplest case of constant phase variation $\beta d = 0$ along the array, the susceptibility response (6) is inherently noncausal and the standard Kramers-Kronig relations do not apply. We have also traced back this noncausality to the polarizability having been concentrated to a point-dipole within each unit cell. It is evident from the previous numerical results, however, that the interaction constant C_{int} in Eq. (6) also plays a role in the noncausal response of the array, affecting the position of the poles Eq. (27). In order to better understand how the point-dipole approximation affects the causality of homogenization models for periodic metamaterial arrays, in this section we derive Eq. (6) from first-principles physical considerations. This allows us to clarify

the limitations of introducing the point-dipole approximation in classic Maxwell-Garnett schemes and discuss how the noncausal features may be avoided by adopting a more rigorous homogenization procedure.

In the context of this paper we use a dynamic homogenization model to derive Eq. (6), analogous to the rigorous homogenization approaches employed in^{12–14} but here applied to the particular case $\beta d = 0$. Under the assumption of zero phase-shift across each unit cell ($\beta d = 0$), the array's electric and magnetic responses are uncoupled and we can rigorously express the effective permittivity as

$$\mathbf{P}_{av} = (\varepsilon_{\text{eff}} - \varepsilon_0)\mathbf{E}_{av}, \quad (28)$$

where the subscript *av* stands for spatial average over one unit cell, applied to the microscopic electric-polarization vector $\mathbf{P}(\mathbf{r})$ and the electric-field vector $\mathbf{E}(\mathbf{r})$. As previously mentioned it is proven in Appendix A that the exact solution to Eq. (28) yields an ε_{eff} that rigorously satisfies causality and the Kramers-Kronig relations.

In order to sustain zero phase shift across the unit cell for finite ω the presence of external sources is required.²⁹ Using an approach analogous to that used in Refs. 12–14, we assume that an external impressed current distribution \mathbf{J}_{ext} is uniformly distributed across the unit cell, sustaining an impressed electric field

$$\mathbf{E}_{\text{ext}} = \mathbf{J}_{\text{ext}}/i\omega\varepsilon_0. \quad (29)$$

Averaging Maxwell's equations over one unit cell, we obtain a general relation between these external sources and the averaged fields

$$i\omega\varepsilon_0(\mathbf{E}_{av} + \mathbf{P}_{av}/\varepsilon_0) = \mathbf{J}_{\text{ext}}, \quad (30)$$

which, combined with Eq. (29), gives

$$\mathbf{E}_{av} = \mathbf{E}_{\text{ext}} - \mathbf{P}_{av}/\varepsilon_0. \quad (31)$$

Introducing the point-dipole approximation, we may relate the induced dipole moment in the unit cell $\mathbf{p} = d^3\mathbf{P}_{av}$ to the local field at its center ($\mathbf{E}_{\text{loc}}^0$) using the polarizability definition

$$\frac{\mathbf{P}_{av}}{\varepsilon_0} = d^{-3}\alpha_e\mathbf{E}_{\text{loc}}^0 = d^{-3}\alpha_e(\mathbf{E}_{\text{array}}^0 + \mathbf{E}_{\text{ext}}), \quad (32)$$

where $\mathbf{E}_{\text{array}}^0$ is the electric field induced at the center of the unit cell by all the other inclusions in the array. $\mathbf{E}_{\text{array}}^0$ is related linearly to \mathbf{P}_{av} as

$$\mathbf{E}_{\text{array}}^0 = d^3C\frac{\mathbf{P}_{av}}{\varepsilon_0}, \quad (33)$$

where $C = \sum_{(l,m,n) \neq (0,0,0)} \mathbf{G}_{ee}(\mathbf{r}_{lmn})e^{-j\beta \cdot \mathbf{r}_{lmn}} \cdot \hat{\mathbf{p}} \cdot \hat{\mathbf{p}}$ and $\mathbf{G}_{ee}(\mathbf{r}_{lmn})$ is the electric dyadic Green's function of the array, assuming that we take into account only the dipolar interactions within the array. Its rapidly converging numerical expression may be found in several recent papers on homogenization of metamaterials.^{7,8,10,12,14} By combining Eqs. (29)–(33), we find that

$$\frac{\mathbf{P}_{av}}{\varepsilon_0} = \frac{1}{d^3(\alpha_e^{-1} - C - d^{-3})}\mathbf{E}_{av}, \quad (34)$$

which coincides with Eq. (6) after defining

$$C_{\text{int}} = C + d^{-3}. \quad (35)$$

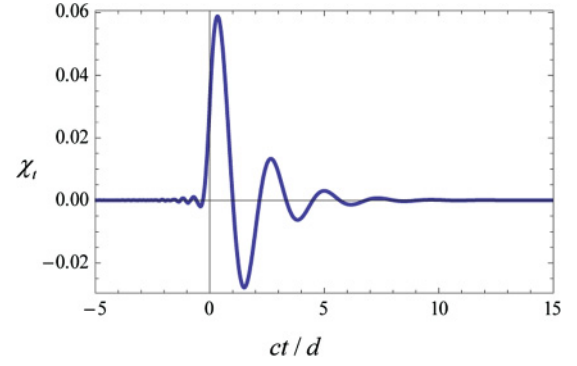


FIG. 6. (Color online) Normalized time response (arbitrary units) of C_{int}^{-1} , which may approximate the array response in the limit of strong scatterers.

The foregoing result is consistent with the more general derivation in Ref. 14.

In the fully dynamic case we have proven that α_e inherently produces a noncausal time advance $\Delta t = -2a/c$ in the time response of \mathbf{P}_{av} produced by $\mathbf{E}_{\text{array}}^0 + \mathbf{E}_{\text{ext}}$ in Eq. (32). In addition C_{int} itself, as defined in Eq. (35), is based on a point-dipole approximation, and it introduces further restrictions on the causal response of the array. This can be seen in the limit of strong scatterers (for instance around the inclusion resonance), for which $\alpha_e \gg C_{\text{int}}^{-1}$ and $\chi_{\text{eff}} \simeq -d^{-3}C_{\text{int}}^{-1}$. Even in this scenario, dual to the one analyzed in Sec. V, the computed time response is inherently noncausal, as shown in Fig. 6 where we plot the inverse Fourier transform of the exact dynamic expression of C_{int}^{-1} . Combining the results in Sections V and VI with these considerations, it is not surprising that the overall response of the susceptibility expression (6), based on point-dipole approximations, is inherently noncausal. More densely packed arrays, for which the time taken to cross one unit cell is of the order of the noncausal time advances introduced by the point-dipole approximations, are more strongly affected and, if conditions (12) are not satisfied, will produce anomalous negative-slope frequency dispersion curves for the effective permittivity. It should not be forgotten, however, that the *time* response will be always noncausal when point-dipole approximations are employed, even when the *frequency* dispersion curves for the effective permittivity have positive slope.

It is interesting to compare these considerations with the full-wave solution obtained when the point-dipole approximation is not applied. In this case the causality of the materials in each unit cell ensures that no microscopic $\mathbf{P}(\mathbf{r}, t)$ can anticipate in time the pulsed-excitation field $\mathbf{E}_{\text{ext}}(t)$, $\beta = 0$. Once established $\mathbf{P}(\mathbf{r}, t)$ induces $\mathbf{E}_{\text{array}}(\mathbf{r}, t)$, but the material causality ensures that $\mathbf{P}_{av}(t)$, $\mathbf{E}_{\text{loc}}(\mathbf{r}, t)$ and $\mathbf{E}_{\text{array}}(\mathbf{r}, t)$ necessarily follow in time the excitation fields $\mathbf{E}_{\text{ext}}(t)$. Since $\mathbf{E}_{av}(t)$ is a unit cell average of $\mathbf{E}_{\text{loc}}(\mathbf{r}, t) + \mathbf{E}_{\text{array}}(\mathbf{r}, t) + \mathbf{E}_{\text{ext}}(t)$, and both $\mathbf{E}_{\text{loc}}(\mathbf{r}, t)$ and $\mathbf{E}_{\text{array}}(\mathbf{r}, t)$ follow in time $\mathbf{E}_{\text{ext}}(t)$, then the exact expression for ε_{eff} in Eq. (28) provides an inherently causal response. This is rigorously proven in Appendix A for microscopic dielectric fields and any fixed β .

Before concluding this section, we point out that the foregoing derivation of Eq. (34) or (6), based on a standard Maxwell-Garnett approach, is not fully consistent with the

assumption of using distributed impressed sources that enforce an $e^{i\beta \cdot r}$ variation in space, required for the Kramers-Kronig relations to hold. This is because the usual expression of α_e in Eq. (32), stemming from Mie theory, implies the usual free-space variation for the exciting fields. To be perfectly consistent with the previous homogenization approach, therefore, in Eq. (32) we should consider a different form of polarizability for the portion of the excitation associated with \mathbf{E}_{ext} , due to the different phase variation of the impressed fields. Although this correction is relatively minor for small k_0d , we have verified that it leads to an intrinsic violation of the passivity condition derived in Sec. IV, and therefore it may produce unwanted artifacts in the effective permittivity. In addition the noncausal features introduced by the point-dipole approximation are still present with this new form of polarizability.

VIII. RESTORING CAUSALITY IN THE HOMOGENIZATION OF METAMATERIALS BASED ON DIPOLAR MODELS

In this section we discuss how the unphysical, noncausal behavior of ε_{eff} associated with the point-dipole approximations, highlighted in Secs. V–VII, can be effectively removed while retaining the advantages of a dipolar description of the array inclusions. We have shown that the dynamic expression for the effective permittivity in a periodic metamaterial array becomes inherently noncausal when point-dipole approximations are used. It is stressed however that in the long-wavelength limit $k_0d \simeq 0$ this approximation is very accurate in describing the dynamic wave interaction within the array, as proven in several recent works on the homogenization of metamaterials.^{10,14} Representing the inclusions as point-dipoles, especially in the case of center-symmetric geometries like spheres, provides excellent agreement with full-wave simulations in predicting the eigen-wave properties and the power relations, such as the absorption and decay rate of the propagating modes, even in the case of very densely packed arrays.¹⁴ Therefore, it may prove beneficial to develop a susceptibility model that retains the point-dipole approximation for the inclusions while restoring a causal response at a fixed value of β .

A first attempt to restore causality within a dipolar approach may simply consist in purposely delaying the polarizability response by a time interval $2a/c$, through defining a modified $\alpha_e(\omega) = \alpha_d(\omega)e^{i\omega 2a/c}$, which was shown in Sec. V to satisfy the Kramers-Kronig relations. Unfortunately this modified polarizability violates the passivity considerations in Sec. IV and thus justifies the appearance of a negative slope in the effective permittivity.

A more rigorous approach may be based on the fact that a strictly causal form of susceptibility must satisfy the Kramers-Kronig relations Eq. (3). In the lossless limit Eq. (6) is purely real, as shown in Sec. III, and its imaginary part, in order to satisfy Eq. (3), is concentrated at the real poles of χ_{eff} :

$$\chi_{\text{eff}}(\omega) = \frac{1}{d^3(\text{Re}[\alpha_e^{-1}] - \text{Re}[C_{\text{int}}])} + i \sum_{\omega_{0i}} \frac{\pi \omega_{\text{pi}}^2}{2\omega_{0i}} \delta(\omega - \omega_{0i}), \quad (36)$$

where ω_{0i} are the poles in the denominator of the first term on the right-hand side of Eq. (36). They are real-valued and represent the natural resonances of the array. The ω_{pi} are arbitrary constants associated with each resonance. Applying Eq. (3), we find

$$\chi'_{\text{eff}}(\omega) = \frac{1}{d^3(\text{Re}[\alpha_e^{-1}] - \text{Re}[C_{\text{int}}])} = \sum_{\omega_{0i}} \frac{\omega_{\text{pi}}^2}{\omega_{0i}^2 - \omega^2}, \quad (37)$$

which implies, as expected, that a causal susceptibility function is required in the lossless limit to be expressed as a sum of causal Lorentzian functions, with poles at real ω_{0i} . In particular Eq. (37) ensures that $-\omega_{\text{pi}}^2/(2\omega_{0i})$ represents the residue associated with a pole at $\omega = \omega_{0i}$. Even when moderate losses are introduced, the effective susceptibility is required to have a similar causal form

$$\chi_{\text{eff}}(\omega) = \sum_{\omega_{0i}} \frac{\omega_{\text{pi}}^2}{\omega_{0i}^2 - 2i\delta_i\omega - \omega^2}, \quad (38)$$

where $\delta_i > 0$ accounts for the presence of finite losses at each resonance.

Eq. (38) implies that a causal form of $\chi_{\text{eff}}(\omega)$ may be obtained by simply extracting the values of ω_{0i} and δ_i at the complex poles $\omega = \sqrt{\omega_{0i}^2 - \delta_i^2} - i\delta_i$ of Eq. (6), that is, the complex roots of the dispersion equation

$$\alpha_e^{-1} - C_{\text{int}} = 0 \quad (39)$$

for a given metamaterial array under its point-dipole approximation. In addition the coefficients ω_{pi} may be obtained as the residues at these poles

$$\omega_{\text{pi}}^2 = -2\sqrt{\omega_{0i}^2 - \delta_i^2} \text{Res}_i. \quad (40)$$

As an additional requirement $\chi_{\text{eff}}(k_0d \rightarrow 0)$ in Eq. (38) has to coincide with the Clausius-Mossotti quasi-static limit (11), yielding the residue summation result

$$\chi_{\text{eff}}(0) = \sum_{\omega_{0i}} \frac{\omega_{\text{pi}}^2}{\omega_{0i}^2}. \quad (41)$$

Consider now, as a first example, the densely packed metamaterial array of Fig. 4, formed by spheres with $\varepsilon = (3 + i0.01k_0d)\varepsilon_0$ and $\gamma = 2.22$. The effective susceptibility dispersion, calculated in Fig. 4, is shown again in Fig. 7 [black line; (a) real part; (b) imaginary part]. As noticed in the previous section, its real part has a negative slope for small k_0d , which violates the causality condition (1b) in this limit of negligible losses, and it is therefore unacceptable on physical grounds. Since we have proven previously that the noncausal portion is associated with a localized anticausal response well represented by a pole along the imaginary axis, we can safely expect that these noncausal features do not significantly affect the imaginary part of $\chi_{\text{eff}}(\omega)$. For this reason using a fitting algorithm we model the dispersion of $\chi''_{\text{eff}}(\omega)$ as a sum of three causal Lorentzian functions, as in Eq. (38). The fitting parameters are given in the first three rows of Table I, and Fig. 7(b) shows that indeed very good matching is achieved between the two curves. The extracted values of ω_{0i} , ω_{pi} , and δ_i are evidently the causal poles and residues of Eq. (39),

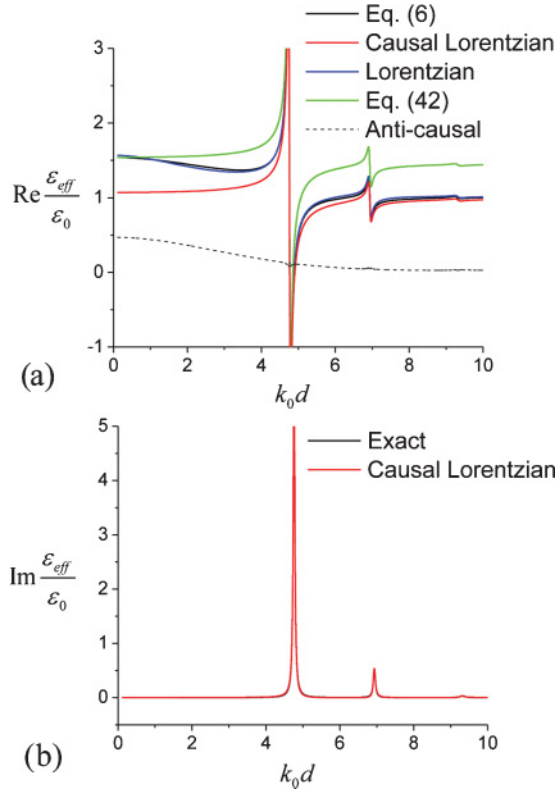


FIG. 7. (Color online) Effective permittivity and different Lorentzian models for a metamaterial array with $\epsilon = (3 + i0.01k_0d)\epsilon_0$ and $\gamma = 2.22$.

and their contribution adequately describes the dispersion of $\chi''_{\text{eff}}(\omega)$ in Fig. 7(b).

The corresponding $\epsilon'_{\text{eff}}(\omega)$, obtained using the retrieved Lorentzian model, is shown as the red line in Fig. 7(a). This permittivity curve is inherently causal and describes to a very good approximation the permittivity dispersion near its resonances and in the higher-frequency regime. However, it dramatically fails to describe the long-wavelength ($k_0d \simeq 0$) response of Eq. (6), and in particular it predicts a static value of $\chi_{\text{eff}}(0)$ that is not consistent with Eq. (41). The difference between the solid curve Eq. (6) and the causal Lorentzian curve is also plotted in Fig. 7(a), as the thin dotted line. This curve effectively extracts the noncausal portion of $\chi_t(t)$, in analogy with the generalized form of the Kramers-Kronig relations in Eq. (20), as the difference between $\chi'_{\text{eff}}(\omega)$ [black curve] and its causal contribution stemming from the usual Kramers-Kronig integral [red]. Consistent with our previous analysis, this curve is well approximated by the presence of one pair of complex conjugate poles along the imaginary axis, perfectly consistent with Eq. (25) (valid for random dilute arrays) and Eq. (27) (valid in the long-wavelength $k_0d \simeq 0$ limit). Indeed, excellent fitting with $\chi'_{\text{eff}}(\omega)$ is obtained with the addition of a simple imaginary pole, as in the fourth row of Table I, which provides the blue line in Fig. 7(a). This pole captures extremely well the anomalous dispersion features of the real part of effective permittivity, over the whole frequency spectrum of interest, and it is associated with the noncausal features produced by the point-dipole approximation, in agreement with our findings in the previous sections. It is evident therefore that

TABLE I. Lorentzian parameters to model the array of Fig. 8 [$\epsilon = (3 + i0.01k_0d)\epsilon_0$, $\gamma = 2.22$].

$\omega_{0r}d/c$	$\omega_{pi}d/c$	$2\delta_i d/c$
4.761	1.211	0.053
6.934	0.5	0.067
9.318	0.229	0.179
2.864 <i>i</i>	2.021 <i>i</i>	0

the contribution to the frequency dispersion from this fourth anticausal pole should be removed to restore causality, still retaining its important role in recovering the correct $\chi_{\text{eff}}(0)$ in Eq. (41).

We can therefore address the causality issue and propose a causal model for the effective permittivity based on a point-dipole description of the array by simply removing the noncausal imaginary pole and artificially adding to the Lorentzian causal permittivity obtained from the dispersion of $\epsilon''_{\text{eff}}(\omega)$ the missing quasistatic contribution $\frac{\omega_{p4}^2}{\omega_{04}^2}$, as shown by the green line in Fig. 7(a). The corrected form of susceptibility effectively becomes

$$\begin{aligned} \chi_{\text{eff}}(\omega) &= \frac{1}{d^3(\alpha_e^{-1} - C_{\text{int}})} - \frac{\omega_{p4}^2}{\omega_{04}^2 - \omega^2} + \frac{\omega_{p4}^2}{\omega_{04}^2} \\ &= \frac{1}{d^3(\alpha_e^{-1} - C_{\text{int}})} + \frac{\omega^2 \omega_{\text{pn}}^2}{\omega_{0n}^2(\omega^2 + \omega_{0n}^2)}, \end{aligned} \quad (42)$$

where $\omega_{0n} = |\omega_{04}|$ and $\omega_{\text{pn}} = |\omega_{p4}|$ refer to the imaginary pole. The causal (green) curve is indeed consistent with the static Clausius-Mossotti homogenization formula (41), it satisfies the causality conditions, and it correctly captures the dynamic resonances of the array, providing a physical description of the array response within its dipolar model.

It should be noted that, for larger frequencies, this corrected form of $\chi_{\text{eff}}(\omega)$ does not tend to zero but to $\omega_{p4}^2/\omega_{04}^2$, and therefore it inherently diverges from the dynamic response of Eq. (6) for short wavelengths and it does not satisfy the expected lack of response for very large frequencies. This is not necessarily unphysical, since we are considering an idealized material with permittivity $\epsilon = (3 + i0.01k_0d)\epsilon_0$. Adopting a causal dispersion model for ϵ that tends to ϵ_0 at large frequencies requires the presence of an additional Lorentzian resonance to restore a causal asymptotic response converging to zero.³⁴ It is irrelevant, however, to consider the applicability of this model for large k_0d , as higher-order multipoles rapidly become more significant. In the long-wavelength regime $k_0d \simeq 0$ of interest here, the corrected model (42), represented by the green line in Fig. 7(a), represents a very good approximation to the exact response of the metamaterial array that restores its causal properties despite the point-dipole approximation.

Figure 8 shows the calculated time response associated with the black and green curves of Fig. 7. In particular the black line represents the time response obtained using Eq. (6), whereas the red line corresponds to the response obtained after suppressing the imaginary pole, using the corrected expression (42). The curves are normalized to the same arbitrary value used in Fig. 5. It is evident that the responses coincide for $t > a/c$, right after the transient regime, and the Lorentzian form

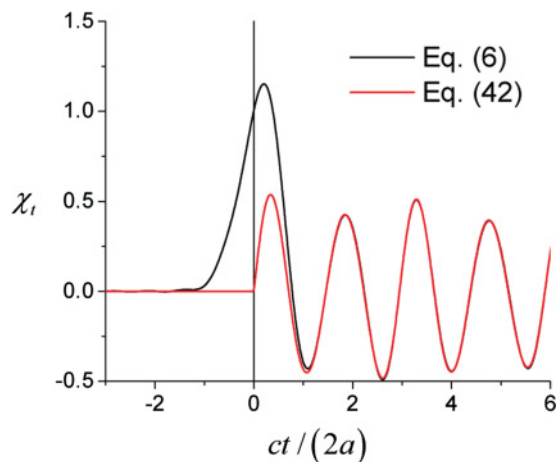


FIG. 8. (Color online) Normalized time response (arbitrary units) associated with the dynamic permittivity model Eq. (6) and the corrected causal response obtained by removing the noncausal pole on the imaginary axis Eq. (42). In this case, $\varepsilon = (3 + i0.01k_0d)\varepsilon_0$ and $\gamma = 2.22$.

of permittivity avoids the noncausal response starting at about $t = -2a/c$, the time advance associated with the point-dipole approximation. This correction is particularly relevant in this example, in which we have considered a very densely packed array violating Eqs. (12), and for which the residue at ω_{04} is large.

We have verified that for less densely packed arrays the proposed correction has a much weaker effect. For instance for a density factor $\gamma = 6.67$, as in the other example of Fig. 4, the correction term in Eq. (42) represents less than a 1.2% correction on the static effective permittivity in Eq. (6). This ensures that, for a less densely packed array satisfying (12), the usual form of susceptibility already has a nearly causal response and effectively no correction is needed. The small noncausality in its time response is still on the order of $t = -2a/c$, as discussed in the previous sections, but in this case it is negligible compared with the time delay introduced by the wave traveling along one array period.

Finally Fig. 9 shows analogous curves for a densely packed array of spheres with $\varepsilon = (20 + i0.1k_0d)\varepsilon_0$ and $\gamma = 2.22$. Here we have extracted five dominant causal poles from the imaginary part of ε_{eff} , as reported in Table II, and an additional noncausal imaginary pole at $\omega_{06} = i2.202$, contributing to the noncausal dispersion represented by the dotted line in Fig. 9(a). Also in this case, anomalous dispersion is accurately described by this imaginary pole, consistent with the previous analysis.

TABLE II. Lorentzian parameters to model the array of Fig. 9 [$\varepsilon = (20 + i0.1k_0d)\varepsilon_0$, $\gamma = 2.22$].

$\omega_{0i}d/c$	$\omega_{pi}d/c$	$2\delta_i d/c$
2.104	0.833	0.02
3.69	0.784	0.065
5.206	0.543	0.12
7.13	0.362	0.202
9.932	0.348	0.255
$2.2i$	$2.544i$	0

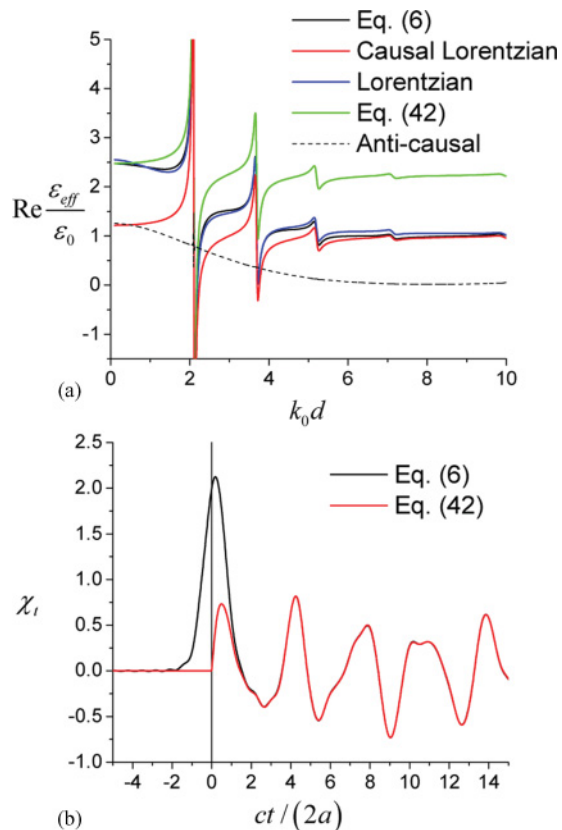


FIG. 9. (Color online) Consistent with Figs. 7 and 8, real part of effective permittivity and time response for an array with $\varepsilon = (20 + i0.1k_0d)\varepsilon_0$ and $\gamma = 2.22$.

The corrected causal response (42), represented by the green line, determines the long-wavelength ($k_0d \simeq 0$) response of the array. The corresponding time response in Fig. 9(b) shows how the two curves extracted from Eqs. (6) and (42) indeed overlap in the steady-state also in this example, and the corrected model ensures a causal transient response. Also in the case of larger permittivity spheres, we have verified that, by reducing the array density, the contribution of the noncausal pole arising from the point-dipole approximation is drastically reduced, and Eq. (42) practically coincides with Eq. (6).

IX. CONCLUSIONS

We have investigated the nature of the noncausality exhibited by the time and frequency responses of homogenized effective (bulk) constitutive parameters of metamaterials. We have shown that a Maxwell-Garnett approach based on point-dipole models, combined with the use of Mie coefficients to describe the inclusion scattering, commonly applied to the homogenization of metamaterials, inherently introduces a noncausal behavior into the effective parameters that violates the standard Kramers-Kronig relations. We have shown, in particular, that the time-domain metamaterial response always starts with a noncausal time advance of the order $\sim 2a/c$, where $2a$ is the inclusion lateral size (for a sphere, its diameter). This small noncausal time advance becomes especially significant in densely packed arrays, for which the time spent by the wave to travel across one unit cell is comparable with this

time advance. We have formulated the general conditions under which anomalous negative-slope dispersion occurs in metamaterial arrays formed by dielectric spheres, we have derived a generalization of the Kramers-Kronig relations that can properly take these noncausal effects into account, and we have discussed a more refined homogenization model, still based on point-dipole approximations, that can correct these noncausal artifacts including the noncausality that can also be associated with positive-slope dispersion. For simplicity we have concentrated our efforts on the special case of $\beta d = 0$. However, similar considerations may be extended to any fixed value of βd . These concepts are particularly important in the case of densely packed metamaterials, violating Eqs. (12), for which standard Maxwell-Garnett homogenization methods should be used with special care. In addition, they provide an understanding of the characteristics, accuracy, and limitations of approximate homogenization models for metamaterials, especially for the anomalous electromagnetic features displayed by densely packed arrays.

ACKNOWLEDGMENTS

This work has been supported in part by the US Air Force Office of Scientific Research through Arje Nachman. A.A. has been supported by an AFOSR YIP Grant No. FA9550-11-1-0009, an NSF CAREER Award No. ECCS-0953311, and an ONR MURI Grant No. N00014-10-1-0942. M.S. has been supported by Fundação para a Ciência e a Tecnologia Grant No. PTDC/EEATEL/100245/2008.

APPENDIX A

In this Appendix, we analytically prove that the full-wave response function of an arbitrary metamaterial array strictly obeys causality and the Kramers-Kronig relations when the detailed microstructure of the unit cell is considered (beyond the point-dipole approximation). Our first goal is to prove that the metamaterial effective susceptibility based on Eq. (28),

$$\mathbf{P}_{\text{av}} = \varepsilon_0 \chi_{\text{eff}} \mathbf{E}_{\text{av}}, \quad (\text{A1})$$

cannot possibly have singularities in the upper half complex ω plane, including the real axis for $\omega \neq 0$, in the presence of finite loss (that can approach zero) for a passive and causal system. Suppose that one such singularity existed for a given (real-valued) wave vector $\boldsymbol{\beta}_0$ at the complex frequency ω_0 , with $\text{Im}[\omega_0] \geq 0$, and imagine the array is excited with the impressed current distribution $\mathbf{J}_{\text{ext}} = \mathbf{J}_0 e^{i\boldsymbol{\beta}_0 \cdot \mathbf{r}}$ with $e^{-i\omega_0 t}$ time dependence. The microscopic fields along the array satisfy

$$\begin{aligned} \nabla \times \mathbf{E}(\mathbf{r}) &= i\omega_0 \mu_0 \mathbf{H}(\mathbf{r}) \\ \nabla \times \mathbf{H}(\mathbf{r}) &= -i\omega_0 \varepsilon_0 \mathbf{E}(\mathbf{r}) - i\omega_0 \mathbf{P}(\mathbf{r}) + \mathbf{J}_{\text{ext}}, \end{aligned} \quad (\text{A2})$$

where (\mathbf{E}, \mathbf{H}) represent the microscopic electric and magnetic fields, and $\mathbf{P} = (\varepsilon - \varepsilon_0)\mathbf{E}$ and $\varepsilon = \varepsilon(\mathbf{r})$ are the local permittivity at frequency ω_0 . (We assume no conduction or magnetic effects in the microscopic features of the array.)

In this general scenario as done in Ref. 12 we define the spatially averaged fields (weighted by $e^{-i\boldsymbol{\beta}_0 \cdot \mathbf{r}}$) as $\mathbf{E}_{\text{av}} = \frac{1}{V} \int_{\text{cell}} \mathbf{E}(\mathbf{r}) e^{-i\boldsymbol{\beta}_0 \cdot \mathbf{r}} dV$, which becomes a simple spatial averag-

ing for $\boldsymbol{\beta}_0 = \mathbf{0}$, as assumed in Sec. VI. Applying this averaging to Eq. (A2) and using (A1) we obtain

$$\begin{aligned} i\boldsymbol{\beta}_0 \times \mathbf{E}_{\text{av}} &= i\omega_0 \mu_0 \mathbf{H}_{\text{av}} \\ i\boldsymbol{\beta}_0 \times \mathbf{H}_{\text{av}} &= -i\omega_0 \varepsilon_0 (1 + \chi_{\text{eff}}) \mathbf{E}_{\text{av}} + \mathbf{J}_0, \end{aligned} \quad (\text{A3})$$

which shows that, under the assumption of χ_{eff} being singular for the given pair $(\omega_0, \boldsymbol{\beta}_0)$, the spatially averaged electric field \mathbf{E}_{av} is required to vanish for a nonzero excitation $\mathbf{J}_0 \neq \mathbf{0}$.

Eq. (A2) implies that

$$\nabla \times \nabla \times \mathbf{E}(\mathbf{r}) - \omega_0^2 \varepsilon(\mathbf{r}) \mu_0 \mathbf{E}(\mathbf{r}) = i\omega_0 \mu_0 \mathbf{J}_{\text{ext}}. \quad (\text{A4})$$

Multiplying both sides of Eq. (A4) by $\mathbf{E}^*(\mathbf{r})$, integrating over one unit cell of the array, and using the fact that $\mathbf{E}_{\text{av}} = \mathbf{0}$ (and thus $\frac{1}{V} \int_{\text{cell}} \mathbf{J}_{\text{ext}} \cdot \mathbf{E}^* dV = \mathbf{J}_0 \cdot \mathbf{E}_{\text{av}}^* = 0$), it follows that for the given pair $(\omega_0, \boldsymbol{\beta}_0)$ associated with the singularity of χ_{eff} , we have

$$\int_{\text{cell}} (|\nabla \times \mathbf{E}(\mathbf{r})|^2 - \omega_0^2 \varepsilon(\mathbf{r}) \mu_0 |\mathbf{E}(\mathbf{r})|^2) dV = 0. \quad (\text{A5})$$

Consider first the special case in which the singular frequency lies along the positive imaginary axis $\omega_0 = i\xi$, with $\xi > 0$. It is well known that $\varepsilon(\mathbf{r}|\omega = i\xi) > \varepsilon_0$ for any passive and causal material,¹⁵ and thus in that case the integrand of Eq. (A5) is the sum of two positive terms that must both vanish for any arbitrary \mathbf{r} . This implies that the assumption of a singular pole along the imaginary axis enforces the trivial solution $\mathbf{E}(\mathbf{r}) = \mathbf{0}$.

Consider now the general case $\omega_0 = \xi e^{i\theta}$ with $0^\circ \leq \theta \leq 180^\circ$. Then Eq. (A5) may be written as $\int_{\text{cell}} (-|\nabla \times \mathbf{E}(\mathbf{r})|^2 e^{-i2\theta} + \xi^2 \varepsilon(\mathbf{r}) \mu_0 |\mathbf{E}(\mathbf{r})|^2) dV = 0$ and, extracting the imaginary part of both sides, it is found

$$\int_{\text{cell}} (|\nabla \times \mathbf{E}|^2 \sin 2\theta + \xi^2 \varepsilon'' \mu_0 |\mathbf{E}|^2) dV = 0, \quad (\text{A6})$$

where $\varepsilon''(\mathbf{r}) = \text{Im}\{\varepsilon(\mathbf{r}|\omega = \xi e^{i\theta})\}$. However, as demonstrated in Appendix B, ε'' has the same sign as the real part of ω , or equivalently it has the same sign as $\sin 2\theta$. Thus, also in this case we can conclude that $\mathbf{E}(\mathbf{r}) = \mathbf{0}$.

We have proven that for any pole of χ_{eff} in the upper-half complex ω plane the microscopic field distribution $\mathbf{E}(\mathbf{r}) = \mathbf{0}$, but this forces \mathbf{J}_{ext} to be zero in Eq. (A4), which in turn contradicts our initial assumption that $\mathbf{J}_0 \neq \mathbf{0}$. In other words we have shown that the response function obtained by averaging over one unit cell the local microscopic fields, as suggested in Refs. 12–14, cannot have singularities in the upper-half plane, including the real axis.

In addition we note that the causality of the material response within the unit cell ensures that $\varepsilon(\mathbf{r}||\omega| \rightarrow \infty) = \varepsilon_0$, that is,

$$\lim_{|\omega| \rightarrow \infty} \mathbf{P}(\mathbf{r}) = \mathbf{0}. \quad (\text{A7})$$

In turn using Eq. (A1), this implies that χ_{eff} is strictly zero on the outer semicircle in the upper-half ω plane for $|\omega| \rightarrow \infty$, and therefore it strictly satisfies all the requirements for the Kramers-Kronig relations for any fixed real-valued wave-vector $\boldsymbol{\beta}$; Q.E.D.

In Fig. 10 we show the comparison between the extracted permittivity curves of Fig. 9 and the full-wave retrieval of

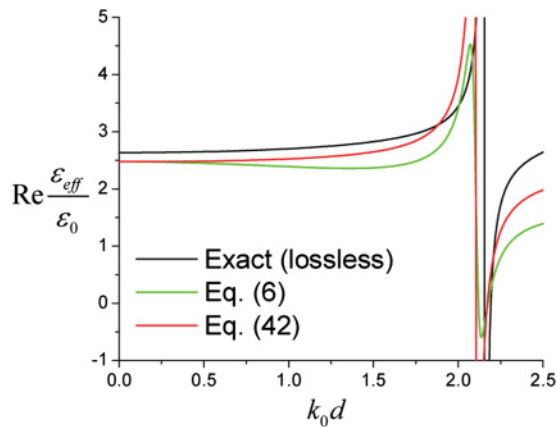


FIG. 10. (Color online) Comparison of the results in Fig. 9 with full-wave FDTD results and Eq. (28) for an array of spheres with $\varepsilon = (20 + i 0.1k_0d)\varepsilon_0$ and $\gamma = 2.22$.

ε_{eff} , obtained using (A1) and a finite-difference-time domain (FDTD) full-wave simulator.³⁶ The exact curve is calculated in the limit of negligible losses (attributable to limitations in the dispersive models available in our FDTD code) and shown as the black curve in Fig. 10. It is seen that the curve has a positive-slope Lorentzian dispersion, analogous to the one predicted by Eq. (42) (red line), which corrects the anomalous negative-slope dispersion in Eq. (6) (green line). Because of the large array packing density, the static result in the full-wave simulations is slightly different from the one predicted by the point-dipole model, as expected because the large capacitance at the gaps between neighboring spheres that are almost touching introduces significant contributions from higher-order multipoles. Despite the large coupling, the first-array resonance is predicted with good accuracy by the point-dipole model, around $k_0d = 2.2$. The corrected model Eq. (42) restores the causality response in the transition between the static result and the first resonance and it avoids the noncausal anomalous dispersion predicted by the point-dipole approximation in Eq. (6), confirming that the approach proposed in Sec. VII effectively restores the causality response

in metamaterial homogenization models based on point-dipole approximations.

APPENDIX B

We demonstrate here that the imaginary part of the permittivity of a causal passive material ε'' has the same sign as the real part of ω for any ω in the upper half-plane. To this end, consider the function $\frac{\Omega \chi(\Omega)}{\Omega^2 - \omega^2}$, where $\text{Im}\{\omega\} > 0$ and $\chi = \varepsilon/\varepsilon_0 - 1$. Integrating this function with respect to Ω on a closed contour of the complex Ω -plane that consists of the real axis and a semicircle of infinite radius in the upper-half plane, then applying the Cauchy integral formula, it is easily shown that

$$\chi(\omega) = \frac{1}{\pi i} \int_{-\infty}^{+\infty} \frac{\Omega \chi(\Omega)}{\Omega^2 - \omega^2} d\Omega. \quad (\text{B1})$$

To obtain the above identity, we used the fact that the integral over the semicircle vanishes and that the integrand has a single pole in the upper-half plane at $\Omega = \omega$. For Ω real valued we can write $\chi(\omega) = \chi'(\omega) + i\chi''(\omega)$, with χ' and χ'' real-valued and possessing even and odd parity, respectively. Hence,

$$\chi(\omega) = \frac{2}{\pi} \int_0^{+\infty} \frac{\Omega \chi''(\Omega)}{\Omega^2 - \omega^2} d\Omega. \quad (\text{B2})$$

This establishes the remarkable result that for ω in the upper-half plane the susceptibility function is completely determined by the values of its imaginary part over the real axis. This result generalizes known results: for instance, for frequencies along the imaginary axis $\omega = i\xi$, Eq. (B2) reduces to the so-called third Kramers-Kronig relation, Eq. (82.15) in Ref. 36. Also, in the limit where $\omega = \omega' + 0^+i$, the formula reduces to the standard Kramers-Kronig relation $\chi'(\omega') = \frac{2}{\pi} P \int_0^{+\infty} \frac{\Omega \chi''(\Omega)}{\Omega^2 - \omega'^2} d\Omega$ because $\frac{1}{\Omega - \omega} = P \frac{1}{\Omega - \omega'} + i\pi\delta(\Omega - \omega')$.

Using Eq. (B2), it is found for $\omega = \omega' + i\omega''$ in the upper-half plane that

$$\chi''(\omega) = \frac{4\omega'\omega''}{\pi} \int_0^{+\infty} \frac{\Omega \chi''(\Omega)}{|\Omega^2 - \omega^2|^2} d\Omega. \quad (\text{B3})$$

Therefore, $\chi'' = \varepsilon''/\varepsilon_0$ has the same sign as ω'' ; Q.E.D.

*alu@mail.utexas.edu

¹N. Engheta and R. W. Ziolkowski, eds., *Electromagnetic Metamaterials: Physics and Engineering Explorations* (John Wiley and Sons, New York, 2006); F. Capolino, ed., *Metamaterials Handbook*, (CRC Press, New York, 2009).

²C. R. Simovski, *Opt. and Spectroscopy* **107**, 726 (2009).

³C. R. Simovski and S. A. Tretyakov, *Phys. Rev. B* **75**, 195111 (2007).

⁴D. R. Smith, *Phys. Rev. E* **81**, 036605 (2010).

⁵A. D. Scher and E. Kuester, *Metamaterials* **3**, 44 (2009).

⁶C. R. Simovski and S. He, *Phys. Lett. A* **311**, 254 (2003).

⁷P. A. Belov and C. R. Simovski, *Phys. Rev. E* **72**, 026615 (2005).

⁸A. Alù and N. Engheta, *Phys. Rev. B* **75**, 024304 (2007).

⁹C. L. Holloway, E. F. Kuester, J. Baker-Jarvis, and P. Kabos, *IEEE Trans. Antennas Propagat.* **51**, 2596 (2003).

¹⁰R. A. Shore and A. Yaghjian, *Radio Sci.* **42**, RS6S21 (2007).

¹¹C. Fietz and G. Shvets, *Physica B* **405**, 2930 (2010).

¹²M. G. Silveirinha, *Phys. Rev. B* **76**, 245117 (2007); M. G. Silveirinha, in *Theory and Phenomena of Artificial Materials, Metamaterials Handbook*, edited by F. Capolino (CRC Press, New York, 2009), Chap. 10, Vol. I.

¹³G. W. Milton, *The Theory of Composites, Cambridge Monographs on Applied and Computational Mathematics* (Cambridge, UK, 2002).

¹⁴A. Alù, *Phys. Rev. B* **84**, 075153 (2011).

¹⁵L. D. Landau, L. P. Pitaevskii, and E. M. Lifshitz, *Electrodynamics of Continuous Media*, 2nd ed., Elsevier, 1984.

- ¹⁶V. M. Agranovich and S. Ginzburg, *Crystal Optics with Spatial Dispersion, and Excitons*, 2nd ed. (Springer, Berlin, 1984).
- ¹⁷A. Sihvola, *Electromagnetic Mixing Formulas and Applications*, (IEE Press, London, 1999).
- ¹⁸A. Alù, *Phys. Rev. B* **83**, 081102(R) (2011).
- ¹⁹M. G. Silveirinha, *Phys. Rev. B* **83**, 165119 (2011).
- ²⁰T. Koschny, P. Markos, D. R. Smith, and C. M. Soukoulis, *Phys. Rev. E* **68**, 065602 (2003).
- ²¹D. R. Smith, D. C. Vier, T. Koschny, and C. M. Soukoulis, *Phys. Rev. E* **71**, 036617 (2005).
- ²²P. M. Valanju, R. M. Walser, and A. P. Valanju, *Phys. Rev. Lett.* **88**, 187401 (2002).
- ²³R. W. Ziolkowski, *Phys. Rev. E* **63**, 046604 (2001).
- ²⁴J. W. Strutt and Lord Rayleigh, *Philosoph. Magaz.* **34**, 177 (1892).
- ²⁵W. Lamb, D. M. Wood, and N. W. Ashcroft, *Phys. Rev. B* **21**, 2248 (1980).
- ²⁶J. K. Lu, *Boundary-Value Problems for Analytical Functions* (World Scientific, New York, 1993).
- ²⁷D. B. Melrose and R. J. Stoneham, *J. Phys. A: Math. Gen.* **10**, 17 (1977).
- ²⁸G. W. Milton, D. J. Eyre, and J. V. Mantese, *Phys. Rev. Lett.* **79**, 3062 (1997).
- ²⁹It should be noted that for source-free arrays, where the propagation vector β is not fixed, but varies with ω , β can become complex in bandgaps and other frequency regions, even though the inclusions are lossless. This implies that the bulk permittivity or permeability can violate (1a), that is have a negative imaginary part in these frequency regions [20], and thus also violate (1b). Therefore, throughout this paper we confine our discussion to fixed real values of the propagation constant β .
- ³⁰A. Alù and N. Engheta, *J. Appl. Phys.* **97**, 094310 (2005).
- ³¹J. Sipe and J. V. Kranendonk, *Phys. Rev. A* **9**, 1806 (1974).
- ³²W. H. Weber and G. W. Ford, *Phys. Rev. B* **70**, 125429 (2004).
- ³³By ‘anti-Lorentzian’ we indicate here ‘anti-resonant’ frequency dispersion associated with a complex pole in the upper complex ω half-plane. This is generally reflected into a Lorentzian resonance with inverted dispersion, which violates Eq. (1b).
- ³⁴A complex permittivity response whose real part is constant with frequency and larger than the one of free-space, as the one used here to model the dielectric material forming the spheres, cannot satisfy the Kramers-Kronig relations because of its non-zero response for infinite frequencies. We implicitly assume here that the real part of permittivity is constant only within the k_0d range of interest and that there is some form of Lorentzian dispersion at much larger frequencies that restores the proper behavior at infinity and Kramers-Kronig relations. This assumption is consistent with the assumption of a linear frequency dispersion of the imaginary part of permittivity in the same k_0d range.
- ³⁵S. A. Tretyakov, *Analytical Modeling in Applied Electromagnetics* (Artech House, London, 2002).
- ³⁶M. G. Silveirinha, *Phys. Rev. B* **83**, 165104 (2011).